This is a repository copy of *Deconvolution of Rashba and Dresselhaus spin-orbit coupling by crystal axis dependent measurements of coupled InAs/GaSb quantum wells*.

White Rose Research Online URL for this paper:
https://eprints.whiterose.ac.uk/138072/

Version: Accepted Version

Deconvolution of Rashba and Dresselhaus spin orbit coupling by crystal axis dependent measurements in InAs/GaSb coupled quantum wells

C. S. Knox[1,2] *, L.H. Li[1], M.C. Rosamond[1], E.H. Linfield[1], C.H. Marrows[2]

[1] *School of Electronic and Electrical Engineering, University of Leeds, Leeds LS2 9JT,*

United Kingdom

[2] *School of Physics and Astronomy, University of Leeds, Leeds LS2 9JT, United Kingdom*

* Corresponding author, Email: py11csk@leeds.ac.uk

Abstract

The Dresselhaus spin orbit interaction is expected to perturb the quantum spin Hall phase predicted to arise within InAs/GaSb coupled quantum wells. As such, to gain a greater understanding of this spin-orbit interaction, the spin orbit coupling in two InAs/GaSb coupled quantum wells, grown along the [001] axis, is investigated along 3 different in-plane crystallographic axes. Due to the crystallographic axis dependence of the Dresselhaus spin orbit coupling, we can deconvolute this coupling from the axis-invariant Rashba spin orbit coupling. We find that the Dresselhaus parameter is robust against an external gate bias and small changes in growth conditions, with an associated Dresselhaus parameter of $(0.20\pm0.07)\times10^{-11}$ eVm being measured across all samples and top gate bias conditions. In addition we show that the asymmetries associated with the coupled quantum well structure, leading to the Rashba spin orbit coupling, are likely to play a dominant role in determining the spin orbit interaction experienced by a quantum spin Hall state as the system is tuned towards charge neutrality.

Introduction

The quantum spin Hall effect (QSHE)[1] is a novel state of matter that is reminiscent of the integer quantum Hall effect[2, 3]. However, instead of a single spin-degenerate edge state dominating transport under an applied external magnetic field (as is observed in the quantum Hall effect), a set of two, spin-filtered, counter-propagating edge states dominate transport in a system with unbroken time-inversion symmetry, with the spin polarisation of these edge states directed out of the plane of the device [4].

In a material that exhibits the QSHE, there exists a bulk band gap that is topologically distinct from the vacuum. In order to bridge this gap, and so connect these topologically non-trivial and trivial regions of space, there must exist a set of gapless edge states, characterised by a Kramers doublet [5]. Due to the topological origin of these edge states, and the spin filtering they provide, the edge states are protected against elastic backscattering, as such scattering events would require a 180º spin-flip.

Two material systems have been predicted to exhibit the QSHE: HgTe/CdTe quantum wells[6] and InAs/GaSb coupled quantum wells[5] . Both materials have exhibited charge transport dominated by helical edge states that are disrupted by the application of an external magnetic field[7, 8], and both have shown existence of some form of spin-polarised edge transport. In HgTe quantum wells, this was demonstrated by the spontaneous generation of a spin-current at the device edge, where the majority of spins are polarised out of the device plane [9]. In InAs/GaSb coupled quantum wells, spin polarised edge transport was also shown through study of Josephson junctions in which the InAs/GaSb was used as a non-superconducting spacer. In this case, devices showed superconducting quantum interference - like behaviour with a doubled periodicity with respect to ordinary Cooper-pair mediated

superconducting quantum interference devices, indicating that not only is transport dominated by edge states, but that there is also some separation of spin-states along each channel edge[10]. In both cases, the interesting topology required for the effect to manifest itself arises from an inverted band gap, where the highest heavy hole valence band is more energetic than the lowest electron conduction band.

HgTe/CdTe and InAs/GaSb both have a zinc-blende crystal structure throughout their active regions, in which bulk inversion symmetry is broken. In addition, the stack structure of the InAs/GaSb coupled quantum well system adds another layer of asymmetry, known as structural inversion asymmetry. These asymmetries induce a potential gradient across the device, giving rise to an internal electric field that current carrying electrons will experience as an effective magnetic field. Such 'magnetic' fields contribute to spin-orbit coupling (SOC), with bulk inversion asymmetry contributing to Dresselhaus SOC, and structural inversion asymmetry contributing to Rashba SOC. Crucially, these internal magnetic fields do not break time-inversion symmetry [11], and so can co-exist with the QSHE[5].

However, as these SOC magnetic fields do not explicitly conserve out-of-plane spin[12], this co-existence leads to a perturbation of the QSHE state[13]. This has been predicted to change the normally completely out-of-plane polarised spins (see Fig. 1(a)) into k-dependent spin-states (Fig. 1(b)), termed generic helical edge states[14, 15]. It is worth noting that generic helical edge states are still protected against elastic backscattering, as this would require a 180º spin-flip [14, 15], as in the unperturbed case. Generic helical edge states do potentially, though, provide a perturbation that would enable easier inelastic backscattering processes, hence disrupting the quantised nature of the conductance in the QSHE.

The Dresselhaus [15] and Rashba [14] SOC terms contribute in different ways to the production of generic helical edge states, making the deconvolution of these two functionally similar parameters of experimental interest. In particular, the k-linear, electron dominated,

Rashba term does not contribute to the disruption of the perfect out-of-plane polarisation, although higher order terms dominated by heavy-holes would be significant[13, 14].

The electric field responsible for the Rashba spin orbit coupling will always lie along the growth direction. Thus, in wafers grown along the [001] axis, it will always be perpendicular to the current, and so the spin-splitting caused by the internal field will have a constant magnitude across all crystallographic axes (see Fig. 1(c)). However, as the crystalline asymmetry, and therefore the electric field that gives rise to the Dresselhaus SOC, is dependent on the crystal structure, the spin splitting field experienced by the current carrying electrons will vary from axis to axis in this case (see Fig. 1(d)) [16, 17]. This angular dependence can thus be used to separate the angle invariant Rashba SOC from the crystal axis dependent Dresselhaus SOC.

Here we report on the relative magnitudes of the Dresselhaus and *k*-linear Rashba SOCs in an InAs/GaSb QHSE candidate in two separate wafers of comparable quality. In one case the transport arises due to a single carrier gas and in the other case both the electron-like carrier density localised in the InAs layer and the hole-like carrier density within the GaSb layer play a significant part in the charge transport. In this way we show that not only is the Dresselhaus parameter constant across all top gate bias conditions, as expected, but it is also robust against small changes in growth conditions. Additionally, the much larger Rashba parameter increases as carriers are depleted from the active region, implying that the internal potential gradient caused by the stack structure is instrumental to the SOC observed.

Experiment

The layer structure of the InAs/GaSb heterostructures is shown in Fig. 2(a), with wafer 2 having a 4 µm, rather than 3 µm, GaSb buffer in an otherwise identical structure. Both wafers were grown by solid source molecular beam epitaxy in the [001] direction on a (100) n$^+$

GaAs substrate, but with Wafer 2 having a slightly lower arsenic over-pressure when compared with Wafer 1 (3.4×10^{-6} mbar, compared with 4.5×10^{-6} mbar) during the InAs growth.

Wafers were patterned into 50 µm wide Hall bars, with 250 µm gaps between probe arms, using optical lithography and wet chemical etching [18], after first depositing Cr/Au ohmic contacts using thermal evaporation. A 30 nm thick Al_2O_3 dielectric was then deposited by atomic layer deposition at 200 ºC on top of the Hall bar, with a Cr/Au top gate electrode subsequently formed using thermal evaporation. An optical micrograph of a typical device is shown in Fig. 2(b). Measurements were undertaken between 0 T and 8 T in a continuous flow helium cryostat at 1.5 K, using standard lock-in techniques, with a source-drain current of 1 µA.

Hall resistance data for each wafer, at zero top gate voltage, are shown in Figs. 3(a) and 3(b). Wafer 1 shows well-quantised quantum Hall plateaux at even-integer multiples of the von Klitzing constant at most field values [19]. In contrast, Wafer 2 shows a slight bending in the low-field Hall trace (>1 T), in addition to plateaux quantised at odd-integer multiples of the von Klitzing constant. The latter is taken to indicate the presence of hybridisation between a 2D electron gas localised in the InAs layer and a 2D hole gas within the active GaSb layer [20] that is not present in Wafer 1. Despite this, both wafers showed transport behaviour dominated by electrons, as indicated by the sign of the low-field (>0.2 T) Hall coefficient. Additionally, all measured samples showed Shubnikov-de Haas (SdH) oscillations that are contained within a single envelope function with a unified temperature dependence up to 10 K (not shown here), from which the effective mass could be extracted [21]. This confirms that the magnetoresistance behaviour is dominated by a single carrier species (electrons) within this regime [21,22]. A summary of the zero top gate bias transport properties for both wafers is displayed in Table I.

Magnetoresistance measurements were then performed for different gate voltages between ±1 V at 1.5 K with the current applied parallel to the [010] crystallographic axis. It is worth noting that once a top gate bias voltage of greater than ±1 V is applied, hysteretic behaviour is observed – the zero top gate bias magnetotransport is then different from the as-cooled state, with SdH oscillations no longer contained in a single envelope function. This is possibly caused by charge traps underneath the quantum well which results in a second carrier contributing to transport. As such, we are unable to tune the system into a charge-neutral state, where topologically non-trivial transport would dominate[8]. Below a ±1 V top gate voltage, however, one can assume that only the carrier density in the InAs layer is being modulated, with all other layers screened from the applied top gate voltage.

A discrete Fourier transform of the observed SdH oscillations, plotted against inverse field was analysed, and two distinct peaks observed at almost all top gate voltages. An example of the oscillations, at gate voltages of 0 V and –1 V, is shown in Fig. 3(c), with the associated discrete Fourier transform presented in Fig. 3(d). We equate the frequencies associated with the two observed peaks to a spin-split carrier density, the higher of which is aligned to the spin-splitting field caused by the SOC within the material [23, 24]. This was repeated across three more devices, along the [100], [110], and [1$\bar{1}$0] crystallographic axes, respectively, and repeated on a similar set of devices from Wafer 2.

Further Analysis and Discussion

Since the SdH oscillations appear to be due to a single carrier species, they can be analysed using the expression: [23]

$$\Omega = \frac{(n^+ - n^-)\hbar^2}{m^*} \cdot \sqrt{\frac{1}{2(n^+ + n^-) - 2(n^+ - n^-)}}, \tag{1}$$

where $n^\pm$ is the carrier density associated with the aligned and anti-aligned peaks respectively, m^* is the effective mass, and Ω is the total SOC parameter.

Above +0.2 V applied top gate voltage, a new set of SdH oscillations with an entirely different envelope function appears, along with an additional peak in the Fourier transform. We take this to be indicative of occupation of a 2nd electron sub-band, and as such, our model for spin-orbit coupling is no longer valid after this point [24], as inter-subband scattering does not conserve spin. As we fill an excited level, inter-subband scattering will begin to play a significant part in the spin relaxation[25], masking the effect of the Rashba and Dresselhaus SOC. Therefore, we neglect data taken at these gate voltages in our analysis.

The SOC parameter, Ω, is plotted in Fig. 4(a) as a function of gate voltage along different crystallographic axes. As illustrated in Figure 1(d), the Dresselhaus spin-splitting field is parallel to the current direction when the current is applied along the [100] and [010] axes, and so should have a negligible effect on the observed spin-splitting [16]. As such, since we find experimentally equal SOC parameters when the current is applied along the [100] and [010] axes, we plot a single set of SOC parameters representing these two axes.

The total SOC parameter increases as the top gate voltage is made more negative for measurements along all crystallographic axes. While there is a small increase in the difference between the carrier densities associated with the spin-orbit field aligned and anti-aligned peaks (i.e. n^+- n^-) in the discrete Fourier transformed SdH oscillations as the top gate voltage becomes more negative, the main reason for this trend appears to be the drop in carrier density associated with depletion of electrons from the InAs layer. This would signify that a greater proportion of the electrons become aligned with the total SOC field as the top gate voltage becomes more negative.

We understand this increase in the SOC parameter with more negative top gate bias by reasoning that the inherent asymmetry associated with the stacked heterostructure will provide some built-in electric field [24, 26], and thus contribute to all terms in the Rashba SOC [16, 27, 28]. Since the intrinsically p-type GaSb is underneath the intrinsically n-type InAs layer[29],

a dipole will be formed across the active layers, with the bottom of the InAs quantum well being more electrically positive than the top. By applying a negative top gate bias voltage and making the top of the stack-structure more negative, the electric field that arises from the applied top gate voltage will enhance the internal field, resulting in the observed behaviour. A schematic diagram of this is shown in Fig. 2 c), where the carrier density within the InAs layer is forced into closer contact with the GaSb layer as the top of the heterostructure is made more negative.

In Fig 4(a), measurements along the [110] axis have a larger SOC parameter compared with measurements along the $\langle 100 \rangle$ axes, with the opposite behaviour being observed for the [1$\bar{1}$0] axis. This is expected, as in the first case the Dresselhaus spin-splitting field will have an additive contribution to the Rashba spin splitting, and in the second case, a subtractive effect. Thus, we can deconvolute these two SOC terms by fitting the crystallographic axis dependence of the total SOC parameter to the following expression [16].:

$$\Omega = \sqrt{\alpha^2 + \beta^2 + 2\alpha\beta\cos 2\theta}, \qquad (2)$$

where α is the total Rashba parameter, β is the total Dresselhaus parameter, and θ is the angle between the direction of the current and the [110] axis. This fit, for the case of zero gate voltage, is shown in Fig. 4(b). As the total SOC parameter, Ω, is experimentally identical for the [100] and [010] axes, there is confidence that the observed values of Ω along the [110] and [1$\bar{1}$0] axes are the maximum and minimum values for Ω, respectively, due to the $\cos(2\theta)$ term in equation (2).

A plot of the two contributions to the total SOC extracted by this method is shown in Figure 4(c) as a function of applied top gate voltage. As expected, the fitted Rashba

parameter matches closely the total SOC observed for the $\langle 100 \rangle$ set of axes, where the Dresselhaus contribution would be expected to be negligible, in the case where the Rashba term makes a dominant contribution to the SOC, as seen in previous studies [16, 30]. The data also fits well to the gate dependences observed along each axes.

The Rashba parameter was calculated to vary between $(0.88\pm0.07)\times10^{-11}$ eVm at 0.2 V applied top gate bias and $(1.78\pm0.07)\times10^{-11}$ eVm at -1.0 V applied bias. This is significant, as typical measurements on InAs quantum wells with a doped underlayer (to supply the structural inversion asymmetry needed for the Rashba SOC) place the maximum measured Rashba parameter to be approximately 1×10^{-11} eVm[16, 26]. We reason that the presence of a GaSb layer integrated into the active portion of the quantum well will induce a greater asymmetry term within the quantum well when compared to dopants that are remote to the transport channel.

The Dresselhaus parameter was calculated to be $(0.20\pm0.07)\times10^{-11}$ eVm for all gate voltages. At zero gate voltage, this would result in a spin-splitting energy due to the Dresselhaus spin orbit coupling of 1.3 ± 0.5 meV [26]. Interestingly, this is close to the predicted value of the splitting due to bulk-inversion asymmetry in HgTe quantum wells and InAs/GaSb coupled quantum wells of 1.6 meV [31, 32].

We repeated these sets of measurements on Wafer 2, in the two-carrier regime, and the results are plotted in Fig. 5. It is worth remarking that although this wafer is in the two-carrier regime, the transport is still electron-dominated, and we are unable to tune through a hybridisation gap. We thus neglect the effect of any sort of topologically non-trivial behaviour or higher order Rashba terms.

Despite the lower effective mass in Wafer 2, as shown in Table I, the Dresselhaus parameter for this wafer, $(0.19\pm0.08)\times10^{-11}$ eVm, was seen to be similar to that obtained in

Wafer 1. The only difference between the two wafers is the elevated Rashba parameter in wafer 2, which we attribute to the greater contribution to the internal electric field from the hole gas within the GaSb layer – a more electrically positive GaSb layer would result in a steeper potential gradient across the coupled quantum well structure, resulting in larger Rashba parameter.

Conclusion

In conclusion, we have investigated the spin-orbit coupling within InAs/GaSb coupled quantum wells along different crystallographic axes in both the single and double carrier, electron dominated regimes. We find that the k-linear Rashba spin orbit coupling is sensitive to top gate bias conditions, and the precise heterostructure growth, and we measure values of the Rashba parameter varying between $(0.88 \pm 0.07) \times 10^{-11}$ eVm and $(1.78 \pm 0.07) \times 10^{-11}$ eVm at 0.2 V and –1.0 V, respectively, in Wafer 1, and $(0.77 \pm 0.08) \times 10^{-11}$ eVm and $(2.00 \pm 0.08) \times 10^{-11}$ eVm at similar top gate voltages in Wafer 2.

On the other hand, the Dresselhaus spin orbit coupling is constant across all top gate voltages. Additionally the Dresselhaus spin orbit coupling seems insensitive to small variations in growth parameters, as our value of $(0.20 \pm 0.07) \times 10^{-11}$ eVm in the single carrier regime aligns well with our measurements in the double carrier regime, together with recent measurements by Beukman et al. on a wafer with a similar stack structure, but where the spin orbit coupling parameters were extracted from fitting the Shubnikov-de Haas oscillations as a function of top gate voltage. [30] However, this method requires the observation of either a high carrier density or an exceptional mobility within the measured quantum well. This enables the observation of many beating modes at an extremely low field due to SOC which are masked to us by the comparatively low mobility [33] of our samples. That being said, the method here explicitly de-convolutes the Rashba and Dresselhaus terms, and extracts the effect of an

applied top gate bias independently. Additionally, the crystallographic axis dependence of the total SOC is clearly shown here.

Recent measurements on strained InAs/GaInSb coupled quantum wells [34] and InAs/GaSb coupled quantum wells mounted on piezoelectric stressors [35] have highlighted the tunability of the hybridisation gap with either applied or growth-related strain effects. In addition, the Dresselhaus and Rashba spin orbit coupling strength in bulk semiconductors are both tunable by applied stress, leading to a deformation of the crystal structure. [36]. This opens up the possibility that the topological behaviour observed in these classes of structures could be significantly modified by strain tuning.

In this work, we have not been able to study spin orbit coupling close to the hybridisation gap, where topological behaviour will begin to have a significant effect on transport. However, we understand that due to the low electron-like carrier density as the hybridisation gap is approached and the resonant behaviour of the sample resistance within a gapped regime, the technique discussed here may not be applicable. In addition, due to the comparable carrier densities of electrons and holes within the heterostructure as the topologically interesting region is approached, additional spin relaxation mechanisms may become apparent [37, 38], independently of the SOC within the material.

Future studies in this regime would, however, provide fascinating insights into the nature of the topological state seen in this class of material. Additionally, the internal electric fields within the material could be engineered, e.g. by swapping positions of the active InAs and GaSb layers or adjusting their carrier densities, enabling tailoring of spin-orbit coupling in the topological regime.

Figures
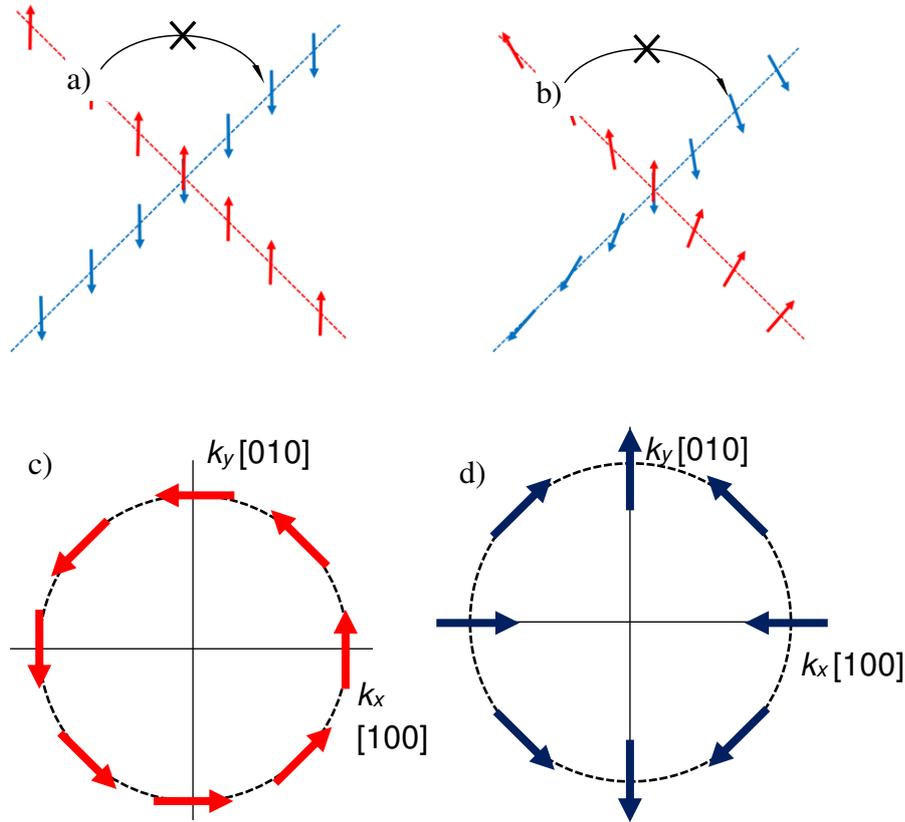
Fig. 1 Schematic $E(k)$ diagram showing (a) an unperturbed helical edge states, and (b) a so-called generic helical edge states[14]. Spin-up states are shown in red and spin down states in blue, with a forbidden elastic backscattering event highlighted (black arrow). Note that to undergo elastic back-scattering in the generic helical regime a 180° spin flip is still required. (c) and (d) show schematics of the 2-D Fermi circle (dotted) showing spin-splitting magnetic fields that arise due to the Rashba spin-orbit coupling (red arrows) , and the Dresselhaus spin-orbit coupling (blue arrows), respectively, for various crystallographic axes.

Wafer	Carrier Density (cm^{-2})	Sheet Mobility (cm^{2}V^{-2}s^{-1})	Effective Mass m$_0$
Wafer 1	$(17.54\pm0.01)\times10^{11}$	111,100±70	0.040±0.005
Wafer 2	$(17.59\pm0.05)\times10^{11}$	137,100±400	0.032±0.005

**Table I**: Table of zero top gate voltage transport parameters for wafer 1 and wafer 2 for current applied along the [100] axis.

	Carrier Density (cm^{-2})	Sheet Mobility (cm^{2}V^{-2}s^{-1})	Effective Mass m$_0$
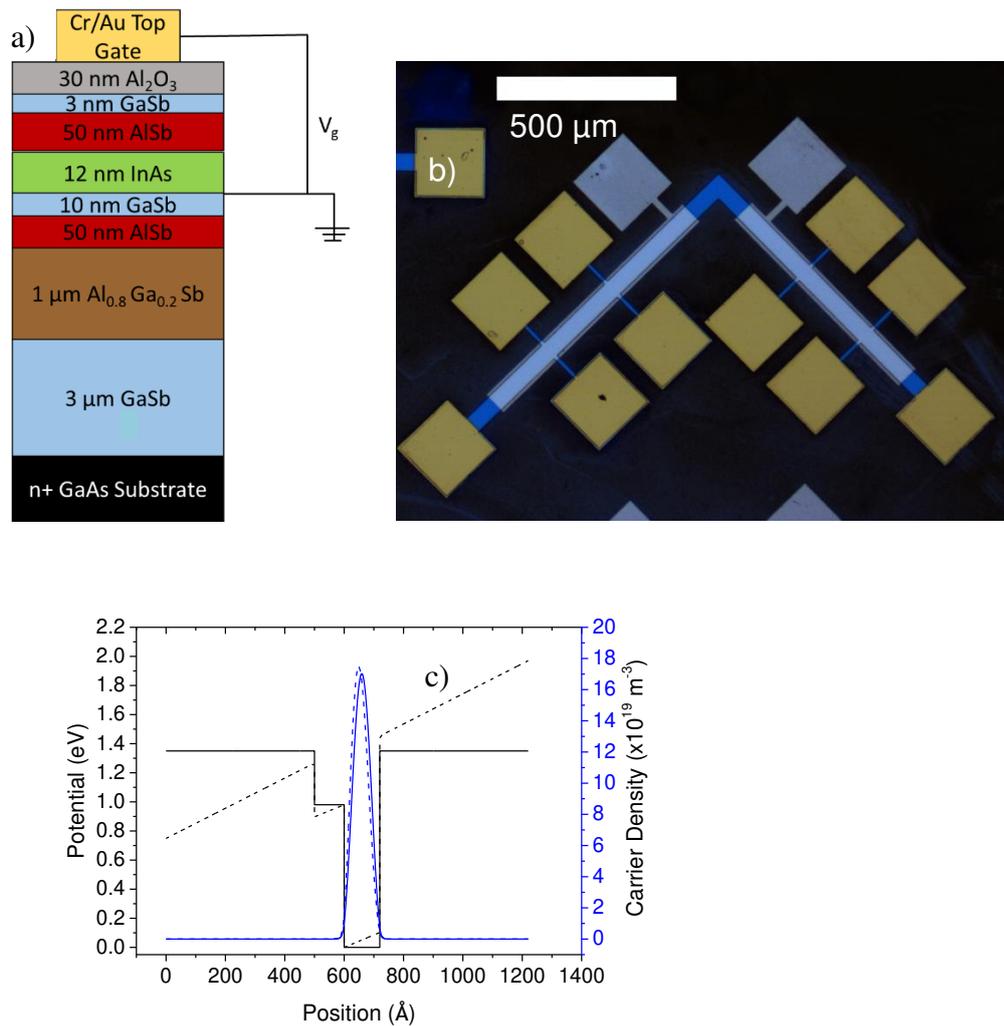
Fig. 2. a) Heterostructure design for Wafer 1; Wafer 2 is identical, except for the use of a 4 μm thick GaSb buffer layer. Note that, since the InAs layer is closer to the top surface, the top gate modulates the electron carrier density. b) Optical micrograph of a typical right-angled Hall bar used in this study. c) Calculated conduction band diagram[39, 40] (black lines) and electron distribution at a fixed carrier density (blue lines) at 0 applied bias (solid lines) and -100 kV/cm electric field, approximately -1 V applied top gate bias (dashed lines). Here, 0 energy is fixed at the bottom of the InAs conduction band.
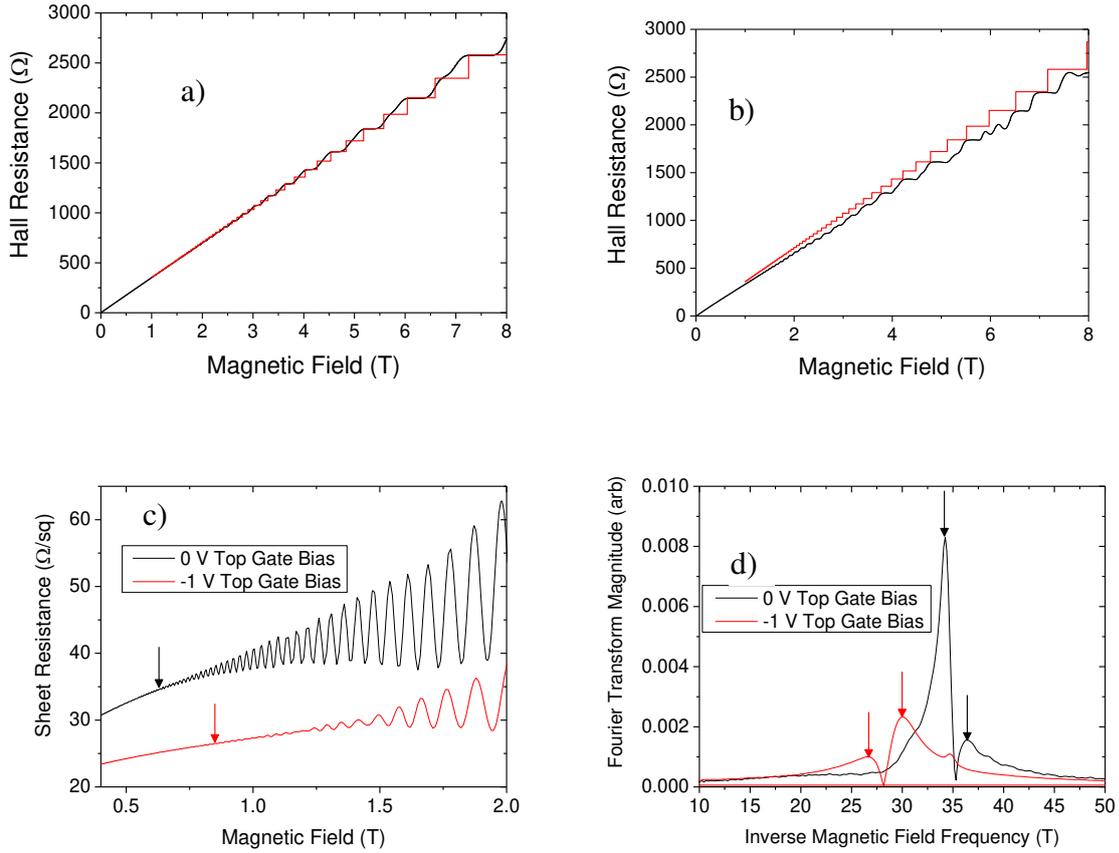
Fig. 3. a) and b) Hall resistance data for Wafers 1 and 2, respectively. The red traces in a) and b) are the expected plateaux arising from the integer quantum hall effect, and are calculated from the low-field (>0.2 T) carrier density. c) SdH oscillations along the [010] axis for Wafer 2 in both the 0 V top gate bias case and with a –1 V applied top gate voltage. Beating nodes, indicating the presence of 2 distinct frequencies, are marked with arrows. d) Discrete Fourier Transform of both sets of oscillations in c), showing two distinct frequencies for each (marked with arrows).
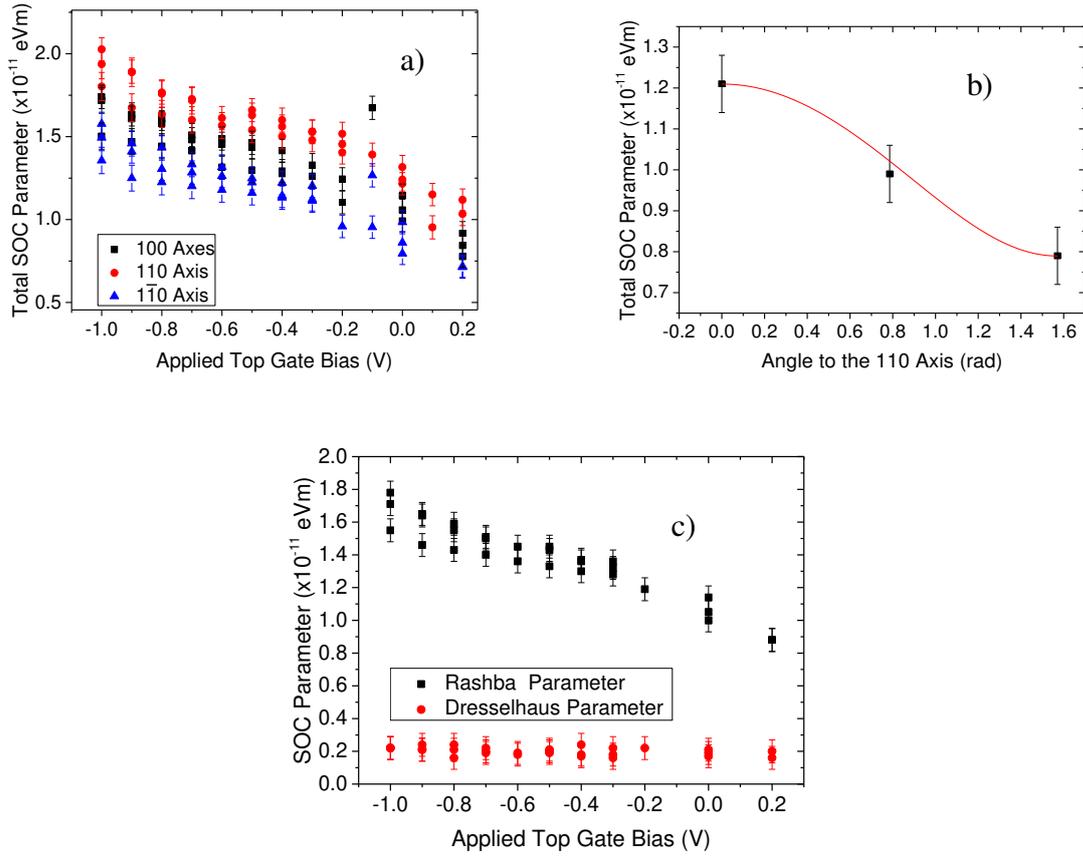
Fig. 4. a) SOC parameters along the [100], [110] and [1$\bar{1}$0] axes of Wafer 1, plotted as a function of top gate voltage. b) Total SOC parameter at zero top gate voltage in Wafer 1, plotted as a function of angle to the [110] axis, showing the expected cos 2θ dependence. The fit to equation (2) is shown in red. c) Rashba and Dresselhaus parameters extracted from fitting equation (2) to the relevant data in Fig. 4 (a).
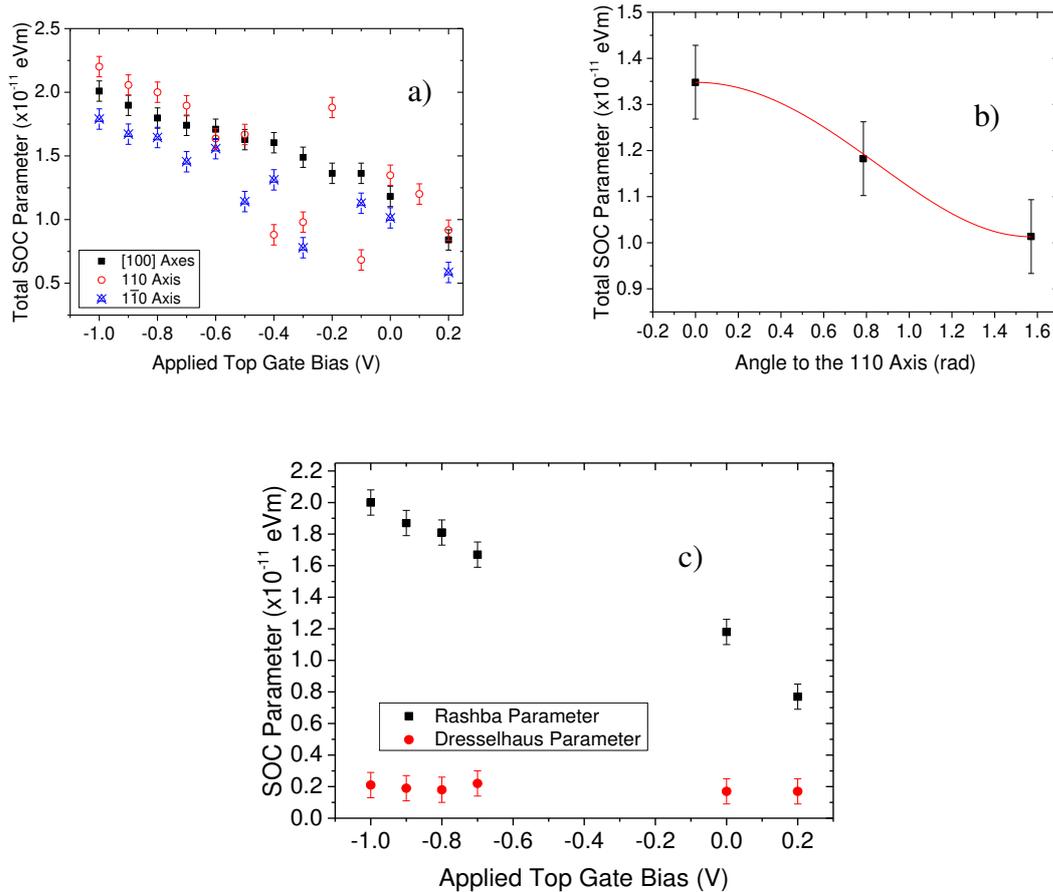
Fig. 5. a) SOC parameters along the [100], [110] and [1$\bar{1}$0] axes of Wafer 2, plotted as a function of top gate voltage. b) Total SOC parameter at zero top gate voltage in Wafer 2, plotted as a function of angle to the [110] axis, showing the expected cos 2θ dependence. The fit to equation (2) is shown in red. c) Rashba and Dresselhaus parameters extracted from fitting equation (2) to the data in the relevant parts of Fig. 5 (a).

References

[1]   C. L. Kane and E. J. Mele, Z(2) topological order and the quantum spin Hall effect, Phys Rev Lett **95** (2005).

[2]   D. J. Thouless, M. Kohmoto, M. P. Nightingale, and M. Dennijs, Quantized Hall Conductance in a Two-Dimensional Periodic Potential, Phys Rev Lett **49**, 405 (1982).

[3]   K. Vonklitzing, G. Dorda, and M. Pepper, New Method for High-Accuracy Determination of the Fine-Structure Constant Based on Quantized Hall Resistance, Phys Rev Lett **45**, 494 (1980).

[4]   C. L. Kane and E. J. Mele, Quantum spin Hall effect in graphene, Phys Rev Lett **95**, 226801 (2005).

[5]   C. X. Liu, T. L. Hughes, X. L. Qi, K. Wang, and S. C. Zhang, Quantum spin Hall effect in inverted Type-II semiconductors, Phys Rev Lett **100**, 236601 (2008).

6   B. A. Bernevig, T. L. Hughes, and S. C. Zhang, Quantum spin Hall effect and topological phase transition in HgTe quantum wells, Science **314**, 1757 (2006).

7   M. Konig, S. Wiedmann, C. Brune, A. Roth, H. Buhmann, L. W. Molenkamp, X. L. Qi, and S. C. Zhang, Quantum spin hall insulator state in HgTe quantum wells, Science **318**, 766 (2007).

8   T. X. Li, et al., Observation of a Helical Luttinger Liquid in InAs/GaSb Quantum Spin Hall Edges, Phys Rev Lett **115**, 136804 (2015).

9   C. Brune, A. Roth, H. Buhmann, E. M. Hankiewicz, L. W. Molenkamp, J. Maciejko, X. L. Qi, and S. C. Zhang, Spin polarization of the quantum spin Hall edge states, Nat Phys **8**, 485 (2012).

10   V. S. Pribiag, A. J. A. Beukman, F. Qu, M. C. Cassidy, C. Charpentier, W. Wegscheider, and L. P. Kouwenhoven, Edge-mode superconductivity in a two-dimensional topological insulator, Nat Nanotechnol **10**, 593 (2015).

11   G. Tkachov and E. M. Hankiewicz, Spin-helical transport in normal and superconducting topological insulators, Phys Status Solidi B **250**, 215 (2013).

12   S. D. Ganichev and L. E. Golub, Interplay of Rashba/Dresselhaus spin splittings probed by photogalvanic spectroscopy - A review, Phys Status Solidi B **251**, 1801 (2014).

13   D. G. Rothe, R. W. Reinthaler, C. X. Liu, L. W. Molenkamp, S. C. Zhang, and E. M. Hankiewicz, Fingerprint of different spin-orbit terms for spin transport in HgTe quantum wells, New J Phys **12**, 065012 (2010).

14   L. Ortiz, R. A. Molina, G. Platero, and A. M. Lunde, Generic helical edge states due to Rashba spin-orbit coupling in a topological insulator, Phys Rev B **93**, 205431 (2016).

15   A. Rod, T. L. Schmidt, and S. Rachel, Spin texture of generic helical edge states, Phys Rev B **91**, 245112 (2015).

16   Y. H. Park, H. J. Kim, J. Chang, S. H. Han, J. Eom, H. J. Choi, and H. C. Koo, Separation of Rashba and Dresselhaus spin-orbit interactions using crystal direction dependent transport measurements, Appl Phys Lett **103**, 252407 (2013).

17   S. D. Ganichev, et al., Experimental separation of Rashba and Dresselhaus spin splittings in semiconductor quantum wells, Phys Rev Lett **92**, 256601 (2004).

18   A. N. Pal, S. Muller, T. Ihn, K. Ensslin, T. Tschirky, C. Charpentier, and W. Wegscheider, Influence of etching processes on electronic transport in mesoscopic InAs/GaSb quantum well devices, Aip Adv **5**, 077106 (2015).

19   S. W. Hwang, H. P. Wei, L. W. Engel, D. C. Tsui, and A. M. M. Pruisken, Scaling in Spin-Degenerate Landau-Levels in the Integer Quantum Hall-Effect, Phys Rev B **48**, 11416 (1993).

20   K. Suzuki, S. Miyashita, and Y. Hirayama, Transport properties in asymmetric InAs/AlSb/GaSb electron-hole hybridized systems, Phys Rev B **67**, 195319 (2003).

21   Y. F. Komnik, V. V. Andrievskii, I. B. Berkutov, S. S. Kryachko, M. Myronov, and T. E. Whall, Quantum effects in hole-type Si/SiGe heterojunctions, Low Temp Phys+ **26**, 609 (2000).

22   C. S. Knox, C. Morrison, F. Herling, D. A. Ritchie, O. Newell, M. Myronov, E. H. Linfield, and C. H. Marrows, Partial hybridisation of electron-hole states in an InAs/GaSb double quantum well heterostructure, Semicond Sci Tech **32**, 104002 (2017).

23   D. Grundler, Large Rashba splitting in InAs quantum wells due to electron wave function penetration into the barrier layers, Phys Rev Lett **84**, 6074 (2000).

24   G. Engels, J. Lange, T. Schapers, and H. Luth, Experimental and theoretical approach to spin splitting in modulation-doped InxGa1-xAs/InP quantum wells for B->0, Phys Rev B **55**, R1958 (1997).

25   H. H. Luo, X. Qian, X. Z. Ruan, Y. Ji, and V. Umansky, Spin dynamics of electrons in the first excited subband of a high-mobility low-density two-dimensional electron system, Phys Rev B **80** (2009).

26   J. Nitta, T. Akazaki, H. Takayanagi, and T. Enoki, Gate control of spin-orbit interaction in an inverted In(0.53)Ga(0.47)AS/In(0.52)Al(0.48)AS heterostructure, Phys Rev Lett **78**, 1335 (1997).

27   G. Gumbs, Rashba effect on the plasma oscillations in a coupled bilayer of electrons and holes, Appl Phys Lett **85**, 2821 (2004).

28   A. H. A. Hassan, R. J. H. Morris, O. A. Mironov, S. Gabani, A. Dobbie, and D. R. Leadley, An origin behind Rashba spin splitting within inverted doped sGe heterostructures, Appl Phys Lett **110**, 042405 (2017).

29   H. Kroemer, The 6.1 angstrom family (InAs, GaSb, AlSb) and its heterostructures: a selective review, Physica E-Low-Dimensional Systems \& Nanostructures **20**, 196 (2004).

30   F. K. d. V. Arjan J. A. Beukman, Jasper van Veen, Rafal Skolasinski, Michael Wimmer,, Spin-orbit interaction in a dual gated InAs/GaSb quantum well, Phys Rev B **96**, 241401 (2017).

31   M. Konig, H. Buhmann, L. W. Molenkamp, T. Hughes, C. X. Liu, X. L. Qi, and S. C. Zhang, The quantum spin Hall effect: Theory and experiment, J Phys Soc Jpn **77**, 031007 (2008).

32   P. C. Klipstein, Structure of the quantum spin Hall states in HgTe/CdTe and InAs/GaSb/AlSb quantum wells, Phys Rev B **91**, 035310 (2015).

33   B. M. Nguyen, W. Yi, R. Noah, J. Thorp, and M. Sokolich, High mobility back-gated InAs/GaSb double quantum well grown on GaSb substrate, Appl Phys Lett **106** (2015).

34   L. J. Du, et al., Tuning Edge States in Strained-Layer InAs/GaInSb Quantum Spin Hall Insulators, Phys Rev Lett **119**, 056803 (2017).

35   L. Tiemann, S. Mueller, Q. S. Wu, T. Tschirky, K. Ensslin, W. Wegscheider, M. Troyer, A. A. Soluyanov, and T. Ihn, Impact of strain on the electronic properties of InAs/GaSb quantum well systems, Phys Rev B **95**, 115108 (2017).

36   B. A. Bernevig and S. C. Zhang, Spin splitting and spin current in strained bulk semiconductors, Phys Rev B **72**, 115204 (2005).

37   J. S. Sandhu, A. P. Heberle, J. J. Baumberg, and J. R. A. Cleaver, Gateable suppression of spin relaxation in semiconductors, Phys Rev Lett **86**, 2150 (2001).

[38] G. L. Bir, A. G. Aronov, and G. E. Pikus, Spin Relaxation of Electrons Scattered by Holes, Zh Eksp Teor Fiz+ **69**, 1382 (1975).

[39] P. Harrison and A. Valavanis, *Quantum wells, wires and dots : theoretical and computational physics of semiconductor nanostructures* (J. Wiley, Chichester, UK, 2016), p. pp 19-81.

[40] C. E. Pryor and M. E. Pistol, Band-edge diagrams for strained III-V semiconductor quantum wells, wires, and dots, Phys Rev B **72** (2005).